

NEAR-WALL TURBULENCE MODIFICATION BY TUNED WALL-IMPEDANCE

Carlo Scalo

Dept. of Mechanical Engineering
Purdue University, USA
scalo@purdue.edu

Julien Bodart

Institut Supérieur de l'Aéronautique et de l'Espace
Université de Toulouse, France
j.bodart@isae.fr

Sanjiva K. Lele

Dept. of Aeronautics & Astronautics,
and Dept. of Mechanical Engineering
Stanford University, USA
lele@stanford.edu

Laurent Joly

Institut Supérieur de l'Aéronautique et de l'Espace
Université de Toulouse, France
laurent.joly@isae.fr

ABSTRACT

We have performed large-eddy simulations of compressible turbulent channel flow at one bulk Reynolds number, $Re_b = 6900$, for bulk Mach numbers $M_b = 0.05, 0.2, 0.5$, with linear acoustic impedance boundary conditions (IBCs), as shown in figure 1. The IBCs are formulated in the time domain following Fung & Ju (2004) and coupled with a fully compressible Navier-Stokes solver. The impedance model adopted is a three-parameter Helmholtz oscillator with resonant frequency tuned to the outer layer eddies. The IBC's resistance, R , has been varied in the range, $R = 0.01, 0.10, 1.00$. Tuned IBCs result in a noticeable drag increase for sufficiently high M_b and/or low R , exceeding 300% for $M_b = 0.5$ and $R = 0.01$, and thus represents a promising passive control technique for delaying boundary layer separation and/or enhancing wall heat transfer. Alterations to the turbulent flow structure are confined to the first 15% of the boundary layer thickness where the classical buffer-layer coherent vortical structures are replaced by an array of Kelvin-Helmholtz-like rollers resulting from a hydro-acoustic instability. The non-zero asymptotic value of the Reynolds shear stress gradient at the wall results in the disappearance of the viscous sublayer and very early departure of the mean velocity profiles from the law of the wall. More details can be found in Scalo *et al.* (2015).

INTRODUCTION

The interaction between a boundary layer and wall-impedance is a classic problem in aeroacoustics. Numerous theoretical investigations by Rienstra and co-workers (Rienstra, 2006; Rienstra & Vilenski, 2008; Rienstra & Darau, 2011; Vilenski & Rienstra, 2007), together with some companion experimental efforts (Boyer *et al.*, 2010), have looked at the stability properties of boundary layers over homogeneous IBCs. In particular, the presence of hydro-acoustic instabilities was predicted under specific conditions, which were deemed to be rarely found in aeronautical practice. Such instability occurs when wall-normal acoustic wave propagation (controlled by the IBCs) becomes hydro-dynamically significant. This type of instability has been

reproduced in the present work, in a fully developed compressible turbulent flow, by *tuning* the characteristic resonant frequency of a mass-spring-damper model for the IBCs (a damped Helmholtz oscillator) to the characteristic hydrodynamic time scale of the flow. While the present results are purely numerical, experimental proof of concept of the proposed flow control strategy has already been successful obtained in the context of laminar flow separation control over an airfoil by Yang & Spedding (2013).

Our approach relies on purely numerical predictions based on high-fidelity fully compressible three-dimensional turbulent simulations, warranting a robust and accurate time-domain formulation of impedance boundary conditions (TDIBCs). TDIBCs require several constraints to be met, which include causality and representation of the boundary as a passive element (Rienstra, 2006). Many physically admissible impedance models have been proposed, with companion strategies for the time-domain formulation. Notable examples include the Extended Helmholtz Resonator model (Richter *et al.*, 2010), the z -transform method (Özyörük & Long, 1997; Özyörük *et al.*, 1998), and the three-parameter model (Tam & Auriault, 1996). Additional challenges are present in their practical numerical implementation, especially when representing external boundaries (Tam, 1998). A mathematically rigorous and effective approach is provided by Fung & Ju (2004), who proposed to apply IBCs indirectly via the reflection coefficient, with special care required in assuring that the causality constraint is met. Fung & Ju (2004)'s strategy has been adopted in the present work and is discussed in detail in the following.

Control of boundary layer turbulence and transition via modified wall-boundary conditions is a topic of formidable research effort. Bodony and co-workers (Zhang & Bodony, 2011; Ostoich *et al.*, 2013) have investigated the interaction of a two-dimensional compressible boundary layer with a single wall-mounted Helmholtz cavity and of a supersonic turbulent boundary layer with a fluttering panel. Tam *et al.* (2013) have simulated a laminar boundary layer developing over an array of resolved wall-mounted Helmholtz resonators. Particular interest is present in the

hypersonic-transition community, where accurate characterization of acoustic properties of ultrasonic absorptive coatings (UAC) has shown to be crucial towards understanding their effects on transition control (Wagner *et al.*, 2014). Bres *et al.* (2013) investigated the stability properties of a two-dimensional hypersonic boundary layer over an idealized porous wall and derived a simple impedance model for companion linear stability calculations. Several high-fidelity numerical simulations have been performed (De Tullio & Sandham, 2010; Wartemann *et al.*, 2012) looking at the interaction between a simplified porous wall geometry and supersonic boundary layers.

The present work investigates the interaction between a damped Helmholtz oscillator model, represented by a three-parameter broadband impedance Tam & Auriault (1996), with fully-developed compressible channel flow turbulence. The goal is to analyze the alterations to the near-wall turbulent structure resulting from the application of tuned wall-impedance in flow configurations previously explored only with impermeable walls (Huang *et al.*, 1995; Coleman *et al.*, 1995; Lechner *et al.*, 2001; Foysi *et al.*, 2004; Ghosh *et al.*, 2010). Relying on high-fidelity three-dimensional fully compressible Navier-Stokes simulations allows to fully capture the nonlinear interactions between wave fluctuations and hydrodynamic events, which characterize the observed flow instability. Moreover, TDIBC implementation strategy adopted provides an exact representation of the acoustic response of a porous surface without the need to resolve its complex geometrical structure. To our knowledge, no previous study has outlined the details of the coupling between TDIBCs and a fully compressible Navier-Stokes solver or has analyzed the structure of a hydro-acoustic instability within a fully developed turbulent flow. The simplicity, uniqueness and relevance of the proposed setup has motivated the present study.

In the following we briefly analyze results from turbulent channel flow coupled with tuned IBCs.

GOVERNING EQUATIONS

All reported quantities are non-dimensionalized with the speed of sound based on the wall temperature, the channel half-width and bulk density (constant for channel flow simulations). The conservation of mass, momentum and specific enthalpy are omitted for the sake of conciseness. The gas is ideal with equation of state $p = \gamma^{-1} \rho T$, and Re and Pr are the Reynolds number and Prandtl number (independent from temperature). A body force is applied in the streamwise direction and adjusted to achieve the desired bulk Mach number, $M_b = \langle \rho u \rangle_\gamma / \langle \rho \rangle_\gamma$ where $\langle \cdot \rangle_\gamma$ is the volume-averaged operator.

The IBCs, no-slip conditions for the tangential velocities and the isothermal conditions

$$\begin{cases} \hat{p} = \pm Z(\omega) \hat{v} & (1a) \\ u = w = 0 & (1b) \\ T = 1, & (1c) \end{cases}$$

respectively, are applied at the walls, $y = \pm 1$, and the impedance $Z(\omega)$ is

$$Z(\omega) = R + i \left[\omega X_{+1} - \omega^{-1} X_{-1} \right], \quad (2)$$

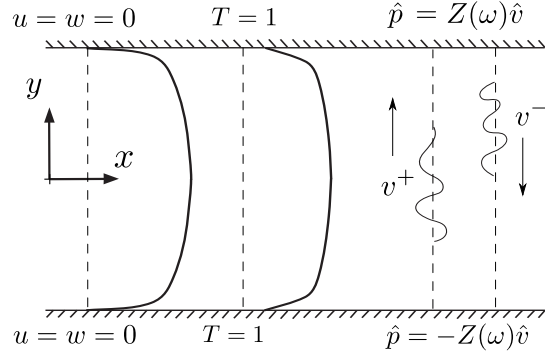


Figure 1. Sketch showing impedance boundary conditions interacting with wall-normal waves in a compressible turbulent channel flow. All quantities shown are non-dimensionalized with the speed of sound based on the wall temperature and the channel half-width. The negative sign for the lower-wall impedance condition is necessary to preserve symmetry. The upper wall is at $y = +1$ and the lower wall is at $y = -1$.

where R is the resistance and the X_{+1} and X_{-1} are the acoustic mass and stiffness, respectively, and ω is the angular frequency. For a given value of the resistance, R , the acoustic mass, X_{+1} , and stiffness, X_{-1} , can be expressed as a function of undamped resonant angular frequency, ω_r , and damping ratio, ζ , based on

$$\begin{cases} \omega_r = \sqrt{X_{-1}/X_{+1}} & (3a) \\ \zeta = \frac{1+R}{2\omega_r X_{+1}}. & (3b) \end{cases}$$

Damping ratios higher than 1 lead to inadmissible (or anti-causal) impedance and, therefore, will not be considered. For a given value of the resistance R , fixing ω_r and ζ in 3 is equivalent to fixing the dimensionless acoustic mass and stiffness in 2 and viceversa. By choosing $Pr = 0.72$ and $n = 0.76$, only five dimensionless parameters are left: two in the governing flow equations, Re (or Re_b) and M_b , and three in the wall impedance, R , X_{+1} , and X_{-1} , or, alternatively, R , ζ , and ω_r .

COMPUTATIONAL SETUP

For the scope of the present study the aforementioned parameter space had to be reduced. For all cases investigated the bulk Reynolds number is fixed to $Re_b = 6900$ in order to obtain a well-developed turbulent flow while maintaining the computational effort manageable. Preliminary numerical trials have shown that tuning of the IBC's undamped resonant angular frequency, ω_r , to the characteristic time scale of the outer scale eddies,

$$\omega_r = 2\pi M_b, \quad (4)$$

results in a noticeable drag increase. While a more systematic analysis on the effects of varying ω_r is deferred to future studies, preliminary numerical investigations show that choosing ω_r to be one order of magnitude larger or smaller than the tuning condition 4 yields to a negligible alteration

of the flow (detuned IBCs). On the other hand, a very similar response to the one observed in the present manuscript was obtained by choosing $\omega_r = 2\pi M_\infty$ where M_∞ is based on the centerline velocity (instead of bulk velocity), showing the robustness of the tuning.

By imposing 4 for all cases, the parameter space is finally reduced to the bulk mach number, M_b , the damping ratio, ζ , and the resistance, R . A set of three values for each parameter has been explored resulting in a total of 27 large-eddy simulations (LES) for all combinations of $M_b = \{0.05, 0.2, 0.5\}$, $\zeta = \{0.5, 0.7, 0.9\}$, and $R = \{0.01, 0.10, 1.00\}$. The chosen values for the resistance bracket the value of 0.18 obtained in Tam & Auriault (1996) by calibrating 2 against the response of a realistic perforated panel. Three additional LES with simple isothermal walls have also been performed for each Mach number to serve as reference cases. More details on the coupling between linear impedance boundary conditions and a fully compressible solver are contained in Scalo *et al.* (2015).

All of the aforementioned exploratory LES are run with respective streamwise and spanwise grid resolutions of $\Delta x^+ < 40$ and $\Delta z^+ < 15$, and with the Vreman (2004) sub-grid scale model active. The computational domain size has been chosen to properly accommodate the near-wall and outer layer turbulent structures in the low-Mach-number limit. A sensitivity study to the grid resolution and domain size has been carried out for the $M_b = 0.5$ and $R = 0.01$ case, which, as discussed in the following, exhibits the strongest response.

The governing equations are solved for mass, momentum and total energy in the finite-volume unstructured code *CharLES^X* developed as a joint-effort project among researchers at Stanford University.

$M_b = 0.05$	$\zeta = 0.50$	$\zeta = 0.70$	$\zeta = 0.90$
$R = 1.00$	0.0 %	0.0 %	0.0 %
$R = 0.10$	1.0 %	1.0 %	1.0 %
$R = 0.01$	75.0 %	127.0 %	134.0 %
$M_b = 0.20$	$\zeta = 0.50$	$\zeta = 0.70$	$\zeta = 0.90$
$R = 1.00$	0.0 %	0.0 %	0.0 %
$R = 0.10$	46.0 %	46.0 %	43.0 %
$R = 0.01$	238.0 %	243.0 %	245.0 %
$M_b = 0.50$	$\zeta = 0.50$	$\zeta = 0.70$	$\zeta = 0.90$
$R = 1.00$	0.0 %	0.0 %	0.0 %
$R = 0.10$	148.0 %	157.0 %	158.0 %
$R = 0.01$	282.0 %	307.0 %	325.0 %

Table 1. Drag increase (%) due to the application of tuned IBC (4) with respect to a baseline case obtained separately for each M_b without IBCs. In all cases the bulk Reynolds number is fixed at $Re_b = 6900$.

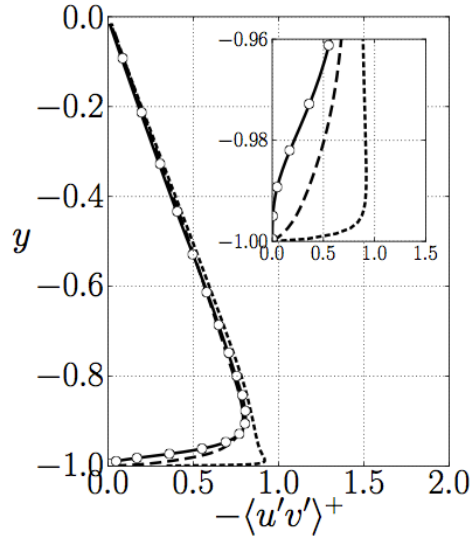


Figure 2. Profiles of resolved Reynolds shear stress for $M_b = 0.2$ and $\zeta = 0.5$. Hard-wall case without IBCs (\circ) plotted every 8 points, $R = 1.00$ (—), $R = 0.10$ (---) and $R = 0.01$ (-.-).

NUMERICAL SIMULATIONS

For sufficiently high Mach numbers, M_b , and low resistances, R , the application of tuned IBCs leads to a strong flow response, in the form of drag increase (table 1). The near-wall streaks disappear and are replaced by quasi periodic arrays of Kelvin-Helmholtz-like rollers (figure 4). Time cross-correlations show that the propagating speed is the local convection velocity, confirming the hydrodynamic nature of the observed instability. The strong similarity between the near-wall spatial structure of wall-normal velocity and pressure fluctuation field suggest that wall-normal wave propagation in the near-wall region is driven (primarily) by acoustic energy exchange mechanisms occurring at the tuned frequency, $\omega_r = 2\pi M_b$. The effects of the wave structure is evanescent in the outer layer. The alternation of the near-wall turbulent structure leads to a significant increase in the Reynolds shear stress near the wall (figure 2). In particular the asymptotic value of Reynolds shear stress gradient near the wall is non-zero, resulting in a departure of the mean velocity profiles from the law of the wall, while second order statistics normalized by friction velocity collapse over different R in the outer layer. This suggest that alterations to the turbulent flow structure remain confined near the wall, in the first 15% of the boundary layer thickness. No quantitative differences in the drag increase and in the altered turbulent structure are observed by changing the grid resolution and domain size separately for the highest Mach number case and the lowest value of the resistance.

The data obtained so far is consistent with an explanation of the observed flow response based on Kelvin-Helmholtz instability mechanisms, as also found in the simulations by Jiménez *et al.* (2001) performed assuming incompressible flow and a purely real impedance at the wall. While Jiménez *et al.* (2001) observes rollers are primarily in the outer layer, modulating the near-wall streaks, in the present investigation (even for $M_b = 0.05$ case), similar structures are present but remain confined near the wall. Moreover, while in Jiménez *et al.* (2001)'s calculations, even at the highest porosities investigated, near-wall streaks

are preserved, in the present case smooth-wall turbulence production mechanisms are completely replaced by Kelvin-Helmholtz-rollers.

Typical buffer-layer turbulent structures are completely suppressed by the application of tuned IBCs. A new *resonance buffer layer* is established characterized by large spanwise-coherent Kelvin-Helmholtz rollers with a well-defined streamwise wavelength, λ_x , traveling downstream with advection velocity $c_x = \lambda_x M_b$. They are the effect of intense hydro-acoustic instabilities resulting from the interaction of high-amplitude wall-normal wave propagation at the tuned frequency $f_r = \omega_r/2\pi = M_b$ with the background mean velocity gradient. The resonance buffer layer is confined near the wall by (otherwise) structurally unaltered outer-layer turbulence. Results suggest that the application of hydrodynamically tuned resonant porous surfaces can be effectively employed in achieving flow control.

LINEAR STABILITY ANALYSIS

In this section, the linear stability analysis of viscous compressible channel flow with impedance boundary conditions is carried out. This method is based on a normal mode analysis of the linearized perturbation equations of Navier-Stokes equations. To find this linearized equation, the instantaneous flow variables are decomposed in a mean and a fluctuating quantity, e.g.

$$u(x, y, t) = \bar{U}(x, y) + u'(x, y, t), \quad (5)$$

where the fluctuating quantity is further expressed as

$$[u', v', p', T']^{\text{tr}} = [\hat{u}(y), \hat{v}(y), \hat{p}(y), \hat{T}(y)]^{\text{tr}} e^{ik(x-ct)} \quad (6)$$

where k is the wave number in x -direction and $\omega = kc$ is the angular frequency. These relations are substituted in the linearized fully compressible Navier-Stokes equation. The resulting eigenvalue problem is solved with a Chebyshev spectral method. To validate the developed code, results are compared against data provided by Hu & Zhong (1998) for viscous compressible Couette flow for which the excellent agreement was observed. Impedance boundary conditions are then applied. The base flow properties are also taken from the LES calculations. Figure 3 (top) shows the eigenvalue spectrum for purely real IBC at $\text{Re}_b = 6900, M_b = 0.5, k = 1, R = 0.01$ using 300 grid points. The two most unstable modes are marked by filled circles. Reynolds stress term computed from perturbed quantities $\overline{u'v'} = \frac{1}{2} [u'v'^*]$ are also plotted for the most unstable mode and qualitatively explain the enhancement of the turbulent Reynolds stresses in the resonance buffer layer as shown in Figure 2.

FUTURE WORK

Further numerical investigations will be pursued at higher Mach numbers ($M_b > 0.5$), where the extreme thinning of the viscous and thermal boundary layers is expected to significantly increase grid resolution requirements. A DNS resolution will be sought for selected cases and turbulent kinetic energy budgets will be extracted, possibly employing a triple decomposition. A scattering model is being investigated in order to explain the interaction between the hydrodynamic and acoustic component of the pressure

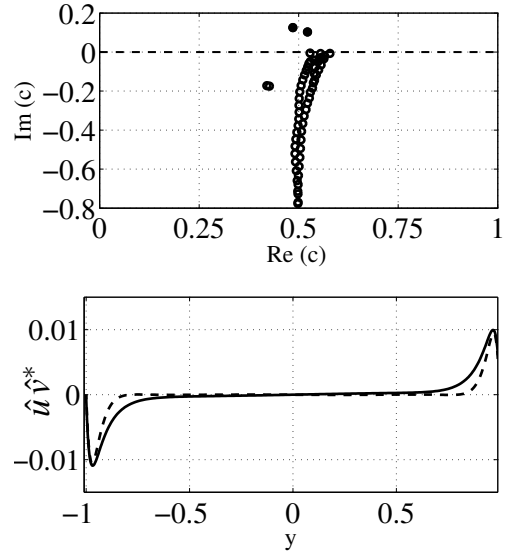


Figure 3. Eigenvalue spectrum (top) and Reynolds stresses (bottom) for compressible channel flow with purely real impedance ($Z(\omega) = R$) at $\text{Re}_b = 6900, M_b = 0.5, R = 0.01$ for perturbation with streamwise wavenumber $k = 1$.

and velocity fields, and the Mach number dependency of the observed flow response. Further work on the linear stability model involves extension of the eigenvalue problem to broadband impedances such as (2). The possibility of realizing companion high-speed tunnel experimental investigations is under consideration.

REFERENCES

- Boyer, G., Piot, E. & Brazier, J.P. 2010 Numerical study of hydrodynamic unstable modes in a ducted shear flow with wall lining and comparison to experiments. In *16th AIAA/CEAS Aeroacoustics Conference*.
- Bres, G. A., Inkman, M., Colonius, T. & Fedorov, A. V. 2013 Second-mode attenuation and cancellation by porous coatings in a high-speed boundary layer. *J. Fluid Mech.* **726**, 312.
- Coleman, G. N., Kim, J. & Moser, R. D. 1995 A numerical study of turbulent supersonic isothermal-wall channel flow. *J. Fluid Mech.* **305** (-1), 159–183.
- De Tullio, N. & Sandham, N. D. 2010 Direct numerical simulation of breakdown to turbulence in a Mach 6 boundary layer over a porous surface. *Phys. Fluids* **22**, 094105.
- Foysi, H., Sarkar, S. & Friedrich, R. 2004 Compressibility effects and turbulence scalings in supersonic channel flow. *J. Fluid Mech.* **509** (-1), 207–216.
- Fung, K. Y. & Ju, H. 2004 Time-domain Impedance Boundary Conditions for Computational Acoustics and Aeroacoustics. *Int. J. Comput. Fluid D.* **18** (6), 503–511.
- Ghosh, Somnath, Foysi, Holger & Friedrich, Rainer 2010 Compressible turbulent channel and pipe flow: similarities and differences. *J. Fluid Mech.* **648**, 155–181.
- Hu, Sean & Zhong, Xiaolin 1998 *Phys. Fluids* **10** (3), 709–730.
- Huang, P. G., Coleman, G. N. & Bradshaw, P. 1995 Compressible turbulent channel flows: DNS results and modelling. *J. Fluid Mech.* **305** (-1), 185–218.
- Jiménez, J., Uhlmann, M., Pinelli, A. & Kawahara, G. 2001

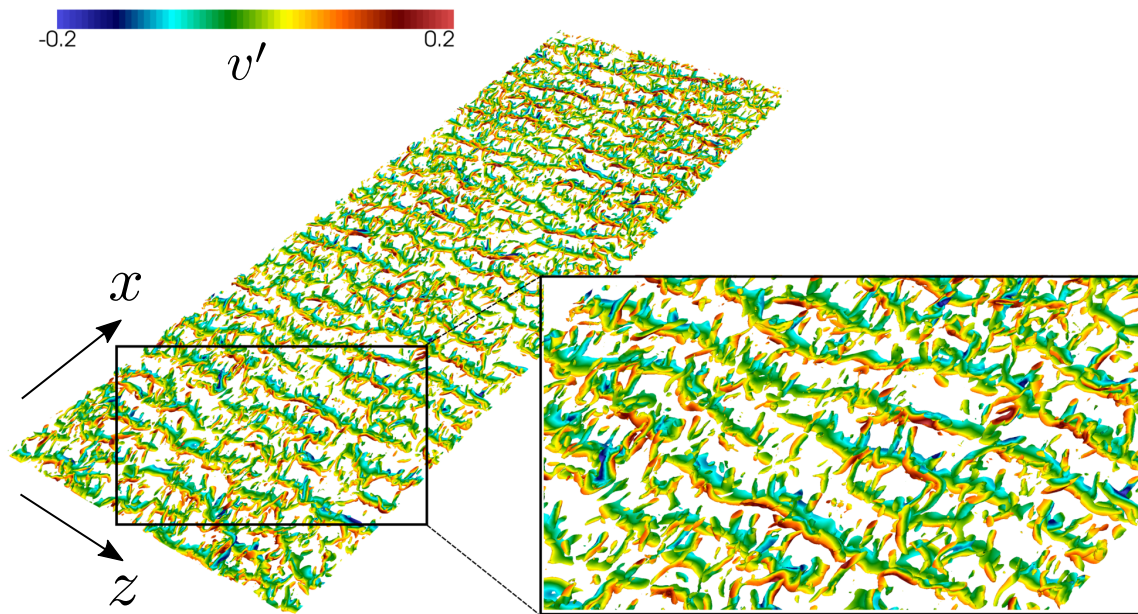


Figure 4. Isosurfaces of second velocity gradient invariant $Q = 5.0$ for $y + 1 < 0.90$ colored by vertical velocity fluctuations for $M_b = 0.5$, $R = 0.01$, $\zeta = 0.5$ on computational domain size $12 \times 2 \times 6$ and resolution equal to $\Delta x^+ = 17$, $\Delta y^+ = 0.3$ (at the wall), $\Delta z^+ = 13$, respectively in the streamwise, wall-normal and spanwise directions.

- Turbulent shear flow over active and passive porous surfaces. *J. Fluid Mech.* **442**, 89–117.
- Lechner, R., Sesterhenn, J. & Friedrich, R. 2001 Turbulent supersonic channel flow. *J. Turbul.* **2**, N1.
- Ostoich, C., Bodony, D. J. & Geubelle, P. H. 2013 Interaction of a Mach 2.25 turbulent boundary layer with a fluttering panel using direct numerical simulation. *Phys. Fluids* **25** (11), 110806.
- Özyörük, Y. & Long, L. N. 1997 A time-domain implementation of surface acoustic impedance condition with and without flow. *J. Comput. Acou.* **5** (3), 277 – 296.
- Özyörük, Y., Long, L. N. & Jones, Michael G. 1998 Time-Domain Numerical Simulation of a Flow-Impedance Tube. *J. Comput. Phys.* **146**, 29 – 57.
- Richter, C., Abdel-Hay, J., Panek, L., Schonwald, N., Busse, S. & Thiele, F. 2010 Time Domain Impedance Modelling and Applications. *Procedia Engineering* **6** (0), 133–142.
- Rienstra, S. W. 2006 Impedance Models in Time Domain, including the Extended Helmholtz Resonator Model. In *12th AIAA/CEAS Aeroacoustics Conference*.
- Rienstra, S. W. & Darau, M. 2011 Boundary-layer thickness effects of the hydrodynamic instability along an impedance wall. *J. Fluid Mech.* **671**, 559 – 573.
- Rienstra, S. W. & Vilenski, G. G. 2008 Spatial instability of boundary layer along impedance wall. In *14th AIAA/CEAS Aeroacoustics Conference*.
- Scalo, C., Bodart, J. & Lele, S. K. 2015 Compressible turbulent channel flow with impedance boundary conditions. *Phys. Fluids* **27** (027503).
- Tam, Christopher K., Pastouchenko, Nikolai, Jones, Michael G. & Watson, Willie R. 2013 *Experimental Validation of Numerical Simulation for An Acoustic Liner in Grazing Flow*.
- Tam, C. K. W. 1998 Advances in numerical boundary conditions for computational aeroacoustics. *J. Comput. Acoust.* **6**, 377–402.
- Tam, C. K. W. & Auriault, L. 1996 Time-domain Impedance Boundary Conditions for Computational Aeroacoustics. *AIAA J.* **34** (5), 917 – 923.
- Vilenski, G. G. & Rienstra, S. W. 2007 On hydrodynamic and acoustic modes in a ducted shear flow with wall lining. *J. Fluid Mech.* **583**, 45–70.
- Vreman, A. W. 2004 An eddy-viscosity subgrid-scale model for turbulent shear flow: Algebraic theory and applications. *Phys. Fluids* **16** (10), 3670.
- Wagner, A., Hannemann, K & Kuhn, M. 2014 Ultrasonic absorption characteristics of porous carbon-carbon ceramics with random microstructure for passive hypersonic boundary layer transition control. *Exp. Fluids* **55**, 1750.
- Wartemann, V., Lüdeke, H. & Sandham, N. D. 2012 Numerical Investigation of Hypersonic Boundary-Layer Stabilization by Porous Surfaces. *AIAA J.* **50**, 1281.
- Yang, S. L. & Spedding, G. R. 2013 Passive separation control by acoustic resonance. *Exp. Fluids* **54**, 1603.
- Zhang, Q. & Bodony, D. J. 2011 Numerical simulation of two-dimensional acoustic liners with high-speed grazing flow. *AIAA J.* **49** (2), 365 – 382.